Article

Degradation of Perfluorooctanoic Acid on Aluminum Oxide Surfaces: New Mechanisms from *Ab Initio* Molecular Dynamics Simulations

Sohag Biswas and Bryan M. Wong*

Read Online

ACCESS | Metrics & More | Article Recommendations | Supporting Information

ABSTRACT: Perfluorooctanoic acid (PFOA) is a part of a large group of anthropogenic, persistent, and bioaccumulative contaminants known as per- and polyfluoroalkyl substances (PFAS) that can be harmful to human health. In this work, we present the first *ab initio* molecular dynamics (AIMD) study of temperature-dependent degradation dynamics of PFOA on (100) and (110) surfaces of γ-Al_2O_3. Our results show that PFOA degradation does not occur on the pristine (100) surface, even when carried out at high temperatures. However, introducing an oxygen vacancy on the (100) surface facilitates an ultrafast (<100 fs) defluorination of C−F bonds in PFOA. We also examined degradation dynamics on the (110) surface and found that PFOA interacts strongly with Al(III) centers on the surface of γ-Al_2O_3, resulting in a stepwise breaking of C−F, C−C, and C−COO bonds. Most importantly, at the end of the degradation process, strong Al−F bonds are formed on the mineralized γ-Al_2O_3 surface, which prevents further dissociation of fluorine into the surrounding environment. Taken together, our AIMD simulations provide critical reaction mechanisms at a quantum level of detail and highlight the importance of temperature effects, defects, and surface facets for PFOA degradation on reactive surfaces, which have not been systematically explored or analyzed.

KEYWORDS: PFAS, thermal degradation, ab initio molecular dynamics, density functional theory, defluorination
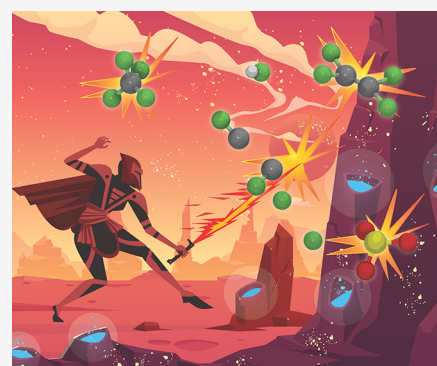
INTRODUCTION

Per- and polyfluoroalkyl substances (PFAS) are artificially made contaminants composed of strong C−F bonds that endow them with exceptional chemical and thermal stability. Because of their intrinsic stability, PFAS have been used in several industries since the 1940s, including packaging materials,[1] cookware,[2] fire-fighting foams,[3] surfactants,[4] and polymers.[5] Due to their widespread use, PFAS contaminants have now been detected in drinking water sources, surface waters, livestock, and agricultural products worldwide.[6] These persistent environmental pollutants are particularly concerning, since chronic exposure to even low concentration levels has been associated with adverse health effects.[7−10] Because of their environmental persistence and negative human and ecological impacts, finding efficient approaches to eliminating these pollutants is essential.

Over the past several years, various oxidation/reduction approaches have been used for PFAS remediation, including hydrated electrons,[11−15] photocatalysis,[16,17] sonochemical oxidation,[18] electrochemical reactions,[19] plasma processes,[20] and UV/sulfite.[21] Recently, calcium-based surfaces have been used for the efficient degradation of perfluorooctanoic acid (PFOA), one type of PFAS, under moderately low temperatures (<1000 °C), which differs from conventional hazardous waste thermal destruction processes that require temperatures

>1000 °C.[22] The calcium surface reduces the formation of perfluorocarbons (a greenhouse gas) by mineralizing the F atoms and, therefore, can be a promising strategy for controlling perfluorocarbon emissions during thermal treatments. Wang et al. further showed that calcium carbonate ($CaCO_3$), calcium oxide (CaO), and calcium hydroxide [$Ca(OH)_2$] can facilitate the destruction of PFAS at temperatures lower than 600 °C.[22−24] Although incineration at temperatures above 500 °C can be a pragmatic approach for eliminating PFAS, these high-temperature processes can produce greenhouse and corrosive gases such as CF_4, C_2F_4, and HF.[24]

While calcium-based surfaces have shown some utility for PFAS destruction, the use of "heavier" metal oxide materials is even more promising since the metal atoms on these thermally stable surfaces have a higher heterogeneity with different coordination/bonding motifs that can further enhance PFAS

degradation. However, due to the inherent complexity of these high-temperature experiments, a detailed understanding of the PFAS degradation mechanisms on these material surfaces is scarce and still in its infancy.[25,26] In this work, we present the first *ab initio* molecular dynamics (AIMD) study for investigating a wide range of temperature-dependent degradation dynamics of perfluorooctanoic acid (PFOA) on various surfaces of γ-Al$_2$O$_3$. We have chosen to investigate γ-Al$_2$O$_3$ since previous work by us and our experimental collaborators[27,28] has shown that γ-Al$_2$O$_3$ has a high degree of surface heterogeneity with Al atoms exhibiting tri-, tetra-, and pentacoordination motifs (depending on the crystallographic plane), which can enhance reactivity. To probe the degradation dynamics of PFOA at a predictive quantum mechanical level, we carried out large-scale AIMD calculations on the (100) and (110) surfaces of γ-Al$_2$O$_3$ (taking into account possible surface defects) over a wide range of temperatures. We give a detailed description of our computational approaches for simulating these complex processes, followed by a variety of analyses of real-time dynamics that explain the underlying mechanisms of the degradation process. Finally, we conclude with a discussion and summary of our results, with additional perspectives of future applications that can have a broad impact in thermal degradation approaches of these environmental contaminants on material surfaces.

■ MATERIAL AND METHODS

Molecular Dynamics Simulations and Optimizations. We carried out Density Functional Theory (DFT)-based *ab initio* molecular dynamics (AIMD) simulations using the CP2K software package.[29] The PBE[30] exchange-correlation functional with Grimme's D3 dispersion correction was used in all of our calculations.[31] We used a DZVP basis set for Al and a TZV2P basis set for the C, O, H, and F valence electrons; Goedecker, Teter, and Hutter (GTH) pseudopotentials were used to treat the atomic core electrons.[32,33] In previous work, we used a similar basis set to accurately simulate the decomposition of diisopropyl methylphosphonate (a chemical warfare agent simulant) on alumina surfaces.[27] The orbital transformation method was used to converge the SCF cycle with an electronic gradient tolerance value of 1×10^{-5} au. The alumina surfaces were optimized with the Broyden–Fletcher–Goldfarb–Shanno (BFGS) minimization algorithm until the forces converged to 4.0×10^{-4} Bohr with an SCF convergence criterion of 1×10^{-5} au. A time step of 0.5 fs with a kinetic energy cutoff of 400 Ry for the auxiliary plane-wave basis was employed to integrate the quantum mechanical equations of motion. All simulations were carried out in a canonical ensemble (NVT) using the Nose–Hoover chain thermostat,[34,35] and several molecular dynamics simulations from 25 to 1200 °C were carried out, as described further below.

Surface Preparation. For our studies, we used the nonspinel model of bulk γ-Al$_2$O$_3$ constructed using crystallographic data by Digne et al.,[36,37] which matches experimental structural parameters (Figure 1a). Our optimized cell parameters (a = 7.90 Å, b = 7.93 Å, and c = 8.07 Å) for bulk alumina are in excellent agreement (deviations less than 2%) with the experimental cell parameters (a = b = 7.96 Å and c = 7.81 Å).[38] The calculations in our study examined the two lowest energy facets (100) and (110) of γ-Al$_2$O$_3$ reported in the scientific literature.[37]

PFOA Degradation Dynamics on the 100 Surface. For our NVT simulations on the (100) surface, we used a single
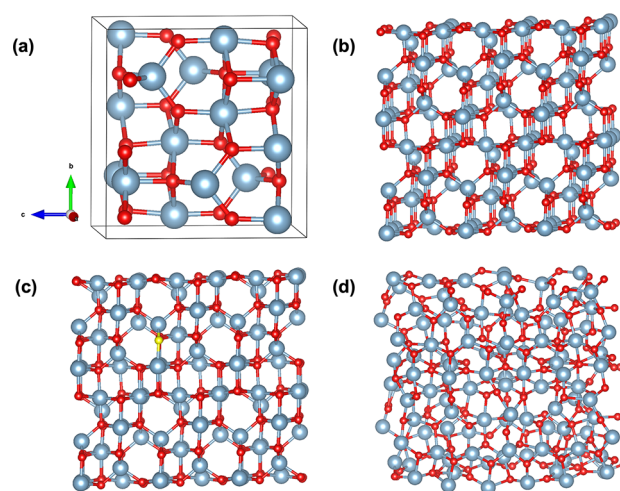

Figure 1. (a) Bulk structure of γ-Al$_2$O$_3$. (b) Optimized geometry of the $3 \times 1 \times 2$ (100) surface of γ-Al$_2$O$_3$. (c) Optimized geometry of the $3 \times 1 \times 2$ (100) surface of γ-Al$_2$O$_3$ with an oxygen defect (shown as a yellow sphere). (d) Optimized geometry of the $2 \times 2 \times 1$ (110) surface of γ-Al$_2$O$_3$.

PFOA molecule and a $3 \times 1 \times 2$ supercell of γ-Al$_2$O$_3$. The PFOA molecule and the atom-numbering scheme used for subsequent analyses in our study are shown in Figure 2, and

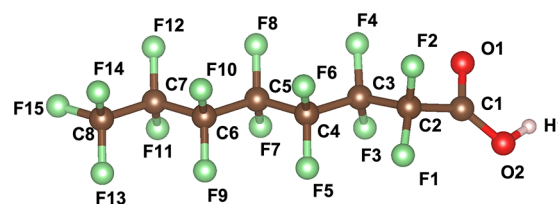**Figure 2.** Chemical structure and atom-numbering scheme of the perfluorooctanoic acid (PFOA) molecule used in our work.

the γ-Al$_2$O$_3$ (100) surface is shown in Figure 1b. To initiate our AIMD simulations, a single PFOA molecule was introduced 4−5 Å above the center of the alumina slab along the *y*-direction. Periodic boundary conditions were applied in the *x* and *z* directions, and a 15 Å vacuum layer was introduced on top of the surface along the *y*-axis. NVT simulations with these initial conditions were carried out at 800, 1000, and 1200 °C. To understand the effect of surface defects on PFOA degradation dynamics, we also carried out AIMD simulations with a defect on the (100) surface of γ-Al$_2$O$_3$, which was created by removing one oxygen atom from the surface, as shown in Figure 1c. NVT simulations for PFOA degradation with this surface defect were performed at 25, 300, 700, 1000, and 1200 °C.

PFOA Degradation Dynamics on the 110 Surface. For our NVT simulations on the (110) surface, we used a single PFOA molecule and a $2 \times 2 \times 1$ supercell of γ-Al$_2$O$_3$. The (110) surface of γ-Al$_2$O$_3$ is shown in Figure 1d. To initiate our AIMD calculations, a single PFOA molecule was introduced 3−4 Å above the center of the alumina slab along the *z*-direction. Periodic boundary conditions were applied in the *x* and *y* directions, and a 15 Å vacuum layer was introduced on top of the surface along the *z*-direction. NVT simulations with these initial conditions were carried out at 25, 300, 700, 1000, and 1200 °C for a total of 5 ps. Previous experimental and theoretical studies have suggested that tricoordinated Al
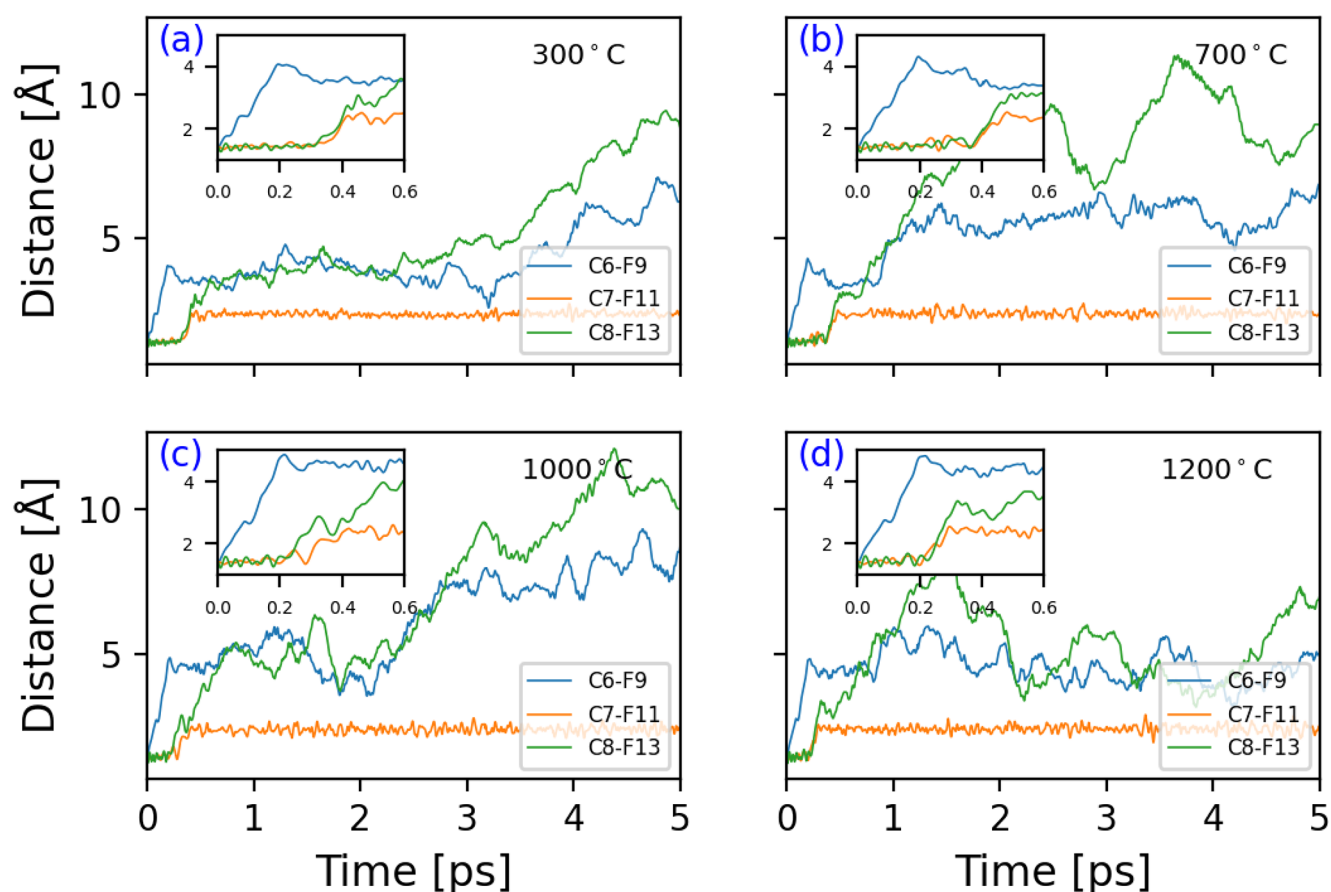
Figure 3. Time-dependent evolution of various C−F bond distances during the defluorination of PFOA on the γ-Al$_2$O$_3$ (100) surface with an oxygen-vacancy defect at various temperatures. The insets in each panel show fluctuations of C−F bond distances up to 600 fs (0.60 ps). The labels in the legend correspond to the atom numbering of the PFOA molecule shown in Figure 2.
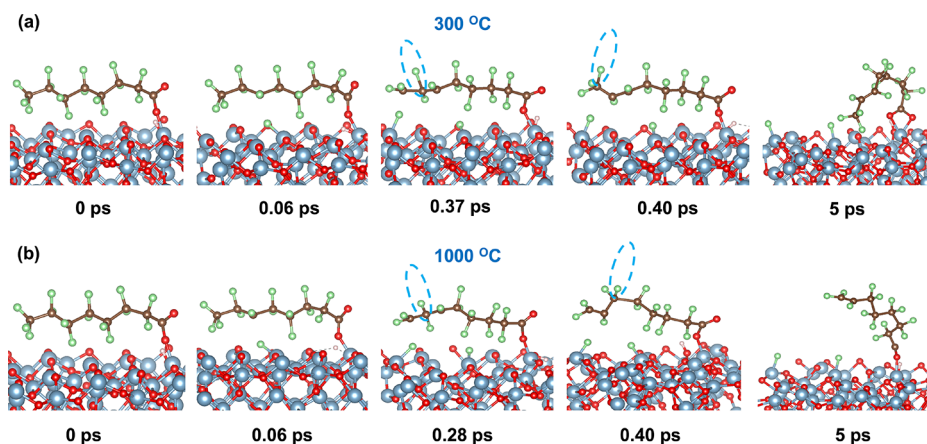

Figure 4. Time-resolved snapshots of representative trajectories illustrate the dissociation of various C−F bonds in PFOA on the γ-Al$_2$O$_3$ (100) surface with an oxygen-vacancy defect. Panels (a) and (b) depict C−F bond dissociation at 300 and 1000 °C, respectively. The dashed oval in panel (a) indicates the migration of the F atom from the C7 (0.37 ps) to the C8 position (0.40 ps), whereas the dashed oval in panel (b) indicates the migration of the F atom from the C7 (0.28 ps) to the C6 position.

centers on a surface play a significant role in catalysis.[36,37,39,40] For example, previous studies of methane activation on the Al$_2$O$_3$ surface indicate that tricoordinated Al enables low-energy pathways for C−H bond splitting.[39,40] It is essential to note that Al(III) centers only exist on the (110) surface and have a higher Lewis acidity than Al(IV).[36,37] In contrast, the (100) surface contains only Al(IV) and Al(V) centers. Since these are the only possible combinations, we only studied the

pristine (110) and oxygen-vacancy (100) surfaces for our PFOA degradation calculations.

■ RESULTS AND DISCUSSION

We first examined the degradation mechanisms of PFOA on a pristine γ-Al$_2$O$_3$ (100) surface at 800, 1000, and 1200 °C. At all of these temperatures, our AIMD calculations show that the PFOA molecule remains largely intact and only loses its acidic
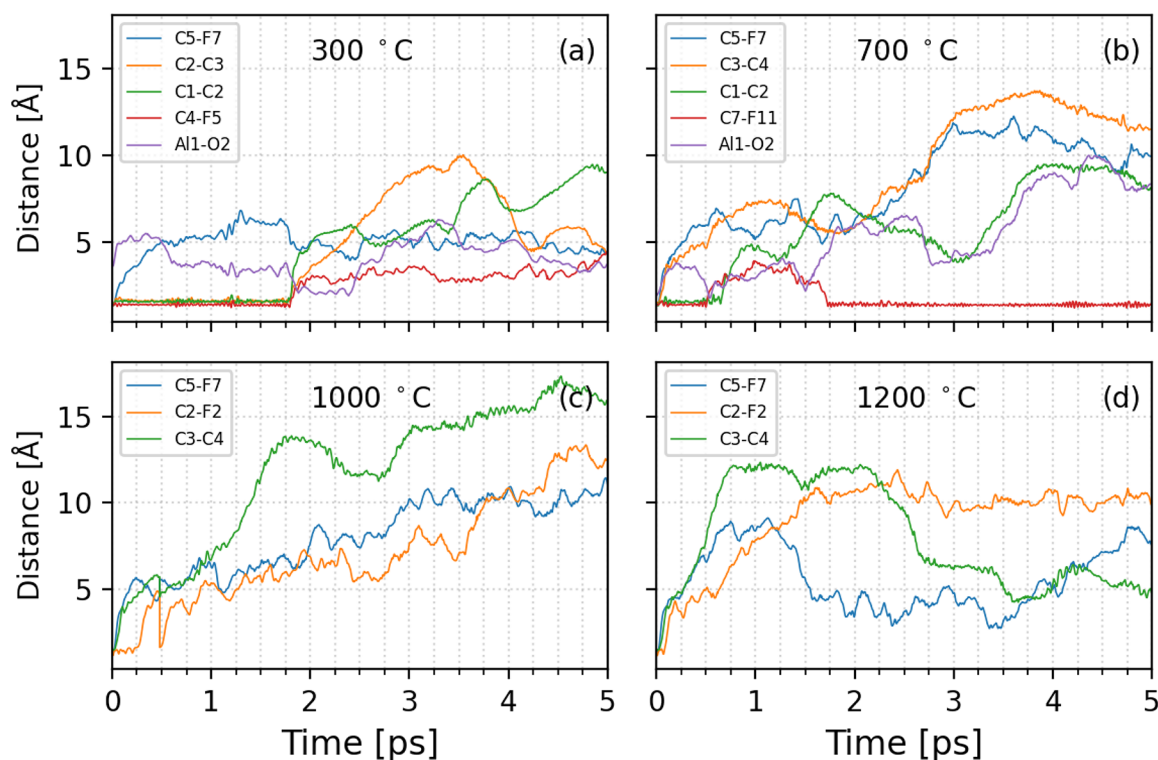
Figure 5. Time-dependent fluctuations of various bond distances during the degradation of PFOA on the γ-Al$_2$O$_3$ (110) surface at various temperatures. The labels in the legend correspond to the atom numbering of the PFOA molecule shown in Figure 2.

hydrogen to the γ-Al$_2$O$_3$ surface as it subsequently adsorbs onto Al atoms at the exposed surface. Figures S1 and S2 in the Supporting Information provide further details of this process by plotting various bond lengths and geometries as a function of time for each of the simulated temperatures. Our AIMD calculations show that even at a relatively high temperature of 1200 °C, the PFOA molecule adsorbs on the alumina surface; however, degradation *does not occur* and none of the F atoms dissociate from the parent molecule.

However, when an oxygen vacancy is introduced on the γ-Al$_2$O$_3$ (100) surface, the degradation dynamics of PFOA are markedly different. Figure 3 summarizes the dissociation dynamics of PFOA on a γ-Al$_2$O$_3$ (100) surface with an oxygen vacancy as a function of time for a few representative temperatures. As the simulations progress, a few of the C−F bonds elongate from ∼1.35 Å (the equilibrium PFOA C−F bond distance) to 3.00 Å and beyond, signifying a complete dissociation. We first observed dissociation of the C6−F9 bond, followed by cleavage of the C7−F11 and C8−F13 bonds. Interestingly, the dissociation of the C6−F9 bond occurs within 100 fs in all these simulations (see the various insets in each panel of Figure 3), indicating an ultrafast degradation that is followed by dissociation of the C7−F11 and C8−F13 bonds.

To further examine the degradation mechanism of PFOA, Figure 4 plots snapshots at critical points for the decomposition of PFOA on the alumina surface for a few representative trajectories at 300 and 1000 °C (snapshots at 700 and 1200 °C are provided in Figure S3 in the Supporting Information). As mentioned in the previous section, the initial decomposition of PFOA occurs via the cleavage of the C6−F9 bond at all temperatures. At 300 °C, Figure 4a depicts a decomposition pathway in which the C6−F9 bond breaks after ∼0.06 ps (60 fs) and an Al−F bond forms with the alumina

surface. At ∼0.37 ps, a single terminal C8−F11 bond is broken when the F11 atom is abstracted by a surface Al(III) atom on alumina and a new Al−F bond is formed. At the same time, the F11 atom (enclosed in a dashed oval for clarity) starts migrating from the C7 to the C8 atom. At 0.40 ps, this migration process is complete and a C═C bond begins to form between the C6 and C7 atoms. Finally, at the end of the AIMD simulation, the C═C bond formation completes, and the PFOA molecule chemically binds to the γ-Al$_2$O$_3$ surface. We also observed a similar degradation mechanism for PFOA at 1000 °C (Figure 4b). However, in this case, migration of the F11 atom occurs from atom C7 to C6, and a C═C bond forms between the C7 and C8 atoms. A similar degradation mechanism is observed for PFOA at 700 and 1200 °C, followed by migration of the F11 atom at the C8 position (see Figure S3 in the Supporting Information). It is worth noting that the formation of Al−F bonds on the γ-Al$_2$O$_3$ surface also reduces secondary pollution since it prevents further dissociation of F$^-$ into water, whose presence can have undesired health effects.[25] Our calculations show that the surface oxygen vacancy promotes the dissociative adsorption of PFOA via cleavage of the C−F bond. These results agree well with related studies on water dissociation on oxygen-defective γ-Al$_2$O$_3$ surfaces.[41] The oxygen vacancy reduces the tetracoordinated Al(IV) center to a tricoordinated Al(III) center, which enhances its Lewis acidic character and enables a stronger attraction between Al(III) and the F atom, thus facilitating C−F dissociation. Static DFT calculations, which do not include thermal effects, have found that the CF$_2$ group at the α position adjacent to the −COOH group is more reactive due to the inductive effect of the headgroup.[13] However, more comprehensive *ab initio* molecular dynamics calculations that incorporate thermal effects by our group have shown that although the α C−F bond is thermodynamically
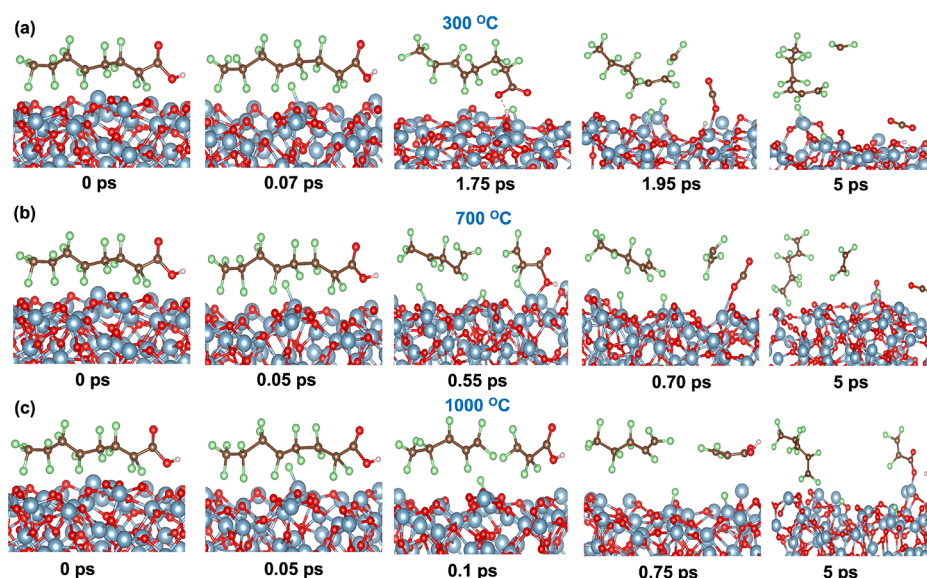
Figure 6. Time-resolved snapshots of representative trajectories illustrate the degradation of PFOA on the γ-Al_2O_3 (110) surface. Panels (a), (b), and (c) depict degradation mechanisms at 300, 700, and 1000 °C, respectively.

more reactive, all other C−F bonds also have a high probability of dissociating in the presence of hydrated electrons.[11] Our present *ab initio* molecular dynamics simulations (which also include thermal effects) suggest that defluorination occurs primarily toward the terminal end of the PFOA chain (the C6, C7, and C8 positions) due to the proximity of the F atoms to the Al(III) centers on the γ-Al_2O_3 (100) surface.

As mentioned earlier, we also studied PFOA degradation on the γ-Al_2O_3 (110) surface, and Figure 5 displays the time-dependent variations of different bond distances. Compared to the (100) surface with an oxygen vacancy, the PFOA degradation mechanisms on the (110) surface are markedly different. At all temperatures $\geq$300 °C, we observed ultrafast dissociation of the C5−F7 bond as well as cleavage of the C−COO and C−C bonds in the PFOA molecule. Figure 5a depicts the dissociation of C−F and C−C bonds in PFOA and the formation of an Al1−O2 bond between the alumina surface and PFOA at 300 °C. At this temperature, both the C1−C2 and C2−C3 bond dissociate in conjunction with another defluorination occurring at the C4 center. We also observed the formation of a bond between the O2 atom of PFOA and an Al(III) atom on the γ-Al_2O_3 surface. Interestingly, our AIMD simulations show a similar time scale for Al1−O2 bond formation, C4−F5 defluorination, and dissociation of C−C bonds, which suggests that the COO$^-$···Al and Al···F interactions activate C−C and C−F bonds. A similar PFOA degradation mechanism is also observed at 700 °C on the γ-Al_2O_3 (110) surface, with the exception that the C1−C2 and C3−C4 bonds dissociate (the C7−F11 bond also dissociates and reforms). At 1000 and 1200 °C, we observed dissociation of only the C3−C4 bond and a second defluorination at the C2 center (see Figure 5c,d).

Figure 6 depicts the degradation mechanism of PFOA on the γ-Al_2O_3 (110) surface at various temperatures. At 300 °C, the F7 atom attached to the C5 center is abstracted by an Al(III) atom on the γ-Al_2O_3 (110) surface (Figure 6a). At ∼1.75 ps, the −COOH group loses its acidic proton to the surface oxygen, and the C3−C4 bond of the PFOA is stretched from its equilibrium bond length. At ∼1.95 ps, one of the oxygen atoms of the −COO group forms a bond with an

Al(III) center, which triggers dissociation of the C1−C2 bond. At the same time, the F5 atom is abstracted by another Al(III) atom from the C4 center, followed by dissociation of the C2−C3 bond. At the end of the simulation, surface-bound CO_2, CF_2, and $CF_3CF_2CF_2CF$=CF−CF_2 fragments are formed with Al−F bonds on the surface. Figure 6b depicts the crucial steps for PFOA degradation at 700 °C on the γ-Al_2O_3 (110) surface. At this temperature, we also observe a similar degradation mechanism; however, the final products are slightly different compared with those observed at 300 °C. Ultrafast dissociation of the C5−F7 bond occurs at ∼0.05 ps (50 fs) as the F atom at the α-position interacts with the Al(III) center. These collective interactions enable the breaking of the C3−C4 bond. In addition, the Al(III) center abstracts the fluorine atom from the C7 position, resulting in defluorination. As the simulation proceeds, a complete decarboxylation happens, and the C1−C2 bond dissociates at ∼0.70 ps. At the end of the reaction, the C7−F11 bond regenerates, resulting in the following reaction products: $CF_3CF_2CF_2CF$=CF_2, CF_2=CF_2, a surface-bound CO_2, and an Al−F bond. At 300 and 700 °C, the PFOA molecule is tightly bound to the γ-Al_2O_3 (110) surface via Al(III)···F and −COO···Al(III) interactions, which weaken the C−F, C−COO, and C−C bonds. These multiple interactions can further enhance and lead to subsequent degradation processes, including decarboxylation, C−C bond scission, and defluorination.[25,26] Figure 6c depicts the PFOA degradation mechanism at 1000 °C where ultrafast dissociation of the C5−F7 bond occurs at 0.05 ps, followed by dissociation of the C3−C4 bond at 0.1 ps. At 0.75 ps, we observe defluorination at the α-position by the surface Al(III) atom and a new Al−F bond is formed. After completion of the reaction at 5 ps, the −COOH group forms a bond with an Al(III) center, resulting in the following degradation products: $CF_3CF_2CF_2CF$=CF_2 and CF_2=CF−COO···Al. A similar degradation mechanism occurs at 1200 °C, which is depicted in Figure S4 in the Supporting Information. In a related study, Wang et al. used an Al_2O_3 catalyst in the presence of a potassium persulfate ball milling agent to degrade PFOA.[25] This study revealed that PFOA initially forms a strong bond with Al via a COO···Al

interaction, resulting in subsequent decarboxylation (via sulfate radicals from the milling agent) and the formation of an unstable C_7F_{15} anion. The C_7F_{15} anion then forms $C_7F_{15}OH$ on the Al_2O_3 surface and undergoes C−F defluorination and cleavage of C−C bonds. Our AIMD calculations also suggest that PFOA degradation occurs on the Al_2O_3 surface by activating C−COO, C−F, and C−C bonds, which corroborates and supports the previous experimental study.

Finally, it is worth mentioning the importance of temperature effects on the degradation dynamics of PFOA on metal oxide surfaces. In particular, we also carried out AIMD calculations at 25 °C on both the (100) and (110) surfaces of γ-Al_2O_3 and found no sign of PFOA degradation at this temperature (see Figures S5−S7 in the Supporting Information). Put differently, *both* the nature of the material facet (i.e., (100)/(110) or pristine/defective) as well as the temperature plays a critical role in the degradation dynamics of PFOA. Conventional static DFT calculations are *unable* to capture the thermal effects required to describe these degradation dynamics; however, these temperature effects are naturally accounted for in our AIMD calculations of PFOA. As such, our quantum dynamics simulations shed crucial mechanistic insight beyond conventional DFT studies into the specific temperatures and facets/defects needed to efficiently degrade these PFOA contaminants.

■ ENVIRONMENTAL IMPLICATIONS

The results of our extensive study have several significant implications for environmental remediation efforts for PFAS contaminants on material surfaces. Thermal treatments at high temperatures can destroy primary PFAS contaminants, but incomplete combustion may result in other undesired secondary byproducts. Often these byproducts can be more volatile than the parent PFAS compounds and still adversely affect the environment and human health. As demonstrated in this work, our predictive AIMD calculations can be used to predict these secondary byproducts and prescreen the conditions required to efficiently remediate these contaminants. In addition, our AIMD calculations indicate that Al_2O_3 offers a new avenue for PFAS degradation at moderately low temperatures (<700 °C) without the costs and complications of flame-based strategies. One particular advantage of this technique is facet engineering, which can enhance PFAS degradation by modulating the reactivity on different facets/surfaces (in addition to temperature effects), as shown by our calculations. Facet engineering is already used in emerging catalysis applications, and our AIMD calculations indicate that these effects should also be leveraged for PFAS remediation efforts. Finally, another significant outcome of our study can be obtained from the inherent statistical nature of PFAS degradation, as demonstrated by our AIMD dynamics calculations. Even though specific C−F bonds might be more thermodynamically reactive, our AIMD simulations show that other C−F bonds in PFOA have a likely probability of dissociating. Therefore, more research efforts should focus on minimizing the contact distance between PFAS molecules and reactive material surfaces rather than merely targeting the weakest C−F bond.

In summary, we have presented the first real-time *ab initio* molecular dynamics study of PFOA degradation on γ-Al_2O_3 to understand the effects of both surface facets and temperature. Our large-scale AIMD calculations show that PFOA degradation does not occur on the pristine γ-Al_2O_3 (100)

surface, even when the reaction is carried out at high temperatures. However, introducing an oxygen vacancy on the (100) surface enables a facile defluorination of C−F bonds and the formation of an alkene-type C=C bond along the PFOA backbone. Our simulations also identified a markedly different degradation mechanism of PFOA on the (110) surface: only C−F bond dissociation occurs on the defected (100) surface; however, dissociation of C−C, C−F, and C−COO bonds all occur on the (110) surface of γ-Al_2O_3. Most importantly, the fluorine atoms on PFOA become mineralized on the Al_2O_3 surface, which can prevent further dissociation of fluorine into the surrounding environment. By explicitly accounting for temperature effects and atomistic details of the surface, our AIMD simulations shed crucial mechanistic insight beyond conventional static DFT calculations (which do not incorporate temperature) into the specific conditions needed to efficiently degrade these PFOA contaminants. Looking forward, our AIMD simulations (1) emphasize the importance of defects and choice of crystallographic surfaces for the degradation of PFOA and (2) highlight the utility of these "beyond-static DFT" dynamical techniques for prescreening candidate surfaces/facets and temperatures to guide experimental efforts in the remediation of PFAS and other environmental contaminants.

■ ASSOCIATED CONTENT

⑤ⁱ Supporting Information

The Supporting Information is available free of charge at https://pubs.acs.org/doi/10.1021/acs.est.3c00948.

> Additional details on the adsorption of PFOA on a pristine γ-Al_2O_3 (100) surface, adsorption and degradation mechanisms on a γ-Al_2O_3 (100) surface with an oxygen-vacancy defect at 700 and 1200 °C, degradation mechanisms of PFOA on a γ-Al_2O_3 (110) surface at 1200 °C, and adsorption of PFOA on the γ-Al_2O_3 (100) and (110) surfaces at 25 °C (PDF)

■ AUTHOR INFORMATION

Corresponding Author

Bryan M. Wong − *Materials Science & Engineering Program, Department of Chemistry, and Department of Physics & Astronomy, University of California—Riverside, Riverside, California 92521, United States;* ⑩ orcid.org/0000-0002-3477-8043; Email: bryan.wong@ucr.edu; http://www.bmwong-group.com

Author

Sohag Biswas − *Materials Science & Engineering Program, Department of Chemistry, and Department of Physics & Astronomy, University of California—Riverside, Riverside, California 92521, United States*

Complete contact information is available at:
https://pubs.acs.org/10.1021/acs.est.3c00948

Notes

The authors declare no competing financial interest.

■ REFERENCES

(1) Schaider, L. A.; Balan, S. A.; Blum, A.; Andrews, D. Q.; Strynar, M. J.; Dickinson, M. E.; Lunderberg, D. M.; Lang, J. R.; Peaslee, G. F. Fluorinated compounds in U.S. fast food packaging. *Environ. Sci. Technol. Lett.* **2017**, *4*, 105−111.

(2) Sajid, M.; Ilyas, M. PTFE-coated non-stick cookware and toxicity concerns: a perspective. *Environ. Sci. Pollut. Res.* **2017**, *24*, 23436−23440.

(3) Guelfo, J. L.; Adamson, D. T. Evaluation of a national data set for insights into sources, composition, and concentrations of per- and polyfluoroalkyl substances (PFASs) in U.S. drinking water. *Environ. Pollut.* **2018**, *236*, 505−513.

(4) Crone, B. C.; Speth, T. F.; Wahman, D. G.; Smith, S. J.; Abulikemu, G.; Kleiner, E. J.; Pressman, J. G. Occurrence of per- and polyfluoroalkyl substances (PFAS) in source water and their treatment in drinking water. *Crit. Rev. Environ. Sci. Technol.* **2019**, *49*, 2359−2396.

(5) Verma, S.; Varma, R. S.; Nadagouda, M. N. Remediation and mineralization processes for per- and polyfluoroalkyl substances (PFAS) in water: a review. *Sci. Total Environ.* **2021**, *794*, 148987.

(6) Lenka, S. P.; Kah, M.; Padhye, L. P. A review of the occurrence, transformation, and removal of poly- and perfluoroalkyl substances (PFAS) in wastewater treatment plants. *Water Res.* **2021**, *199*, 117187.

(7) Lau, C.; Thibodeaux, J. R.; Hanson, R. G.; Narotsky, M. G.; Rogers, J. M.; Lindstrom, A. B.; Strynar, M. J. Effects of perfluorooctanoic acid exposure during pregnancy in the mouse. *Toxicol. Sci.* **2006**, *90*, 510−518.

(8) Brown, J. B.; Conder, J. M.; Arblaster, J. A.; Higgins, C. P. Assessing human health risks from per- and polyfluoroalkyl substance (PFAS)-impacted vegetable consumption: a tiered modeling approach. *Environ. Sci. Technol.* **2020**, *54*, 15202−15214.

(9) Sznajder-Katarzyńska, K.; Surma, M.; Cieślik, I. A review of perfluoroalkyl acids (PFAAs) in terms of sources, applications, human exposure, dietary intake, toxicity, legal regulation, and methods of determination. *J. Chem.* **2019**, *2019*, 1.

(10) Beach, S. A.; Newsted, J. L.; Coady, K.; Giesy, J. P. *Reviews of environmental contamination and toxicology: continuation of residue reviews*; Springer: New York, NY, 2006; pp 133−174.

(11) Biswas, S.; Yamijala, S. S. R. K. C.; Wong, B. M. Degradation of per- and polyfluoroalkyl substances with hydrated electrons: a new mechanism from first-principles calculations. *Environ. Sci. Technol.* **2022**, *56*, 8167−8175.

(12) Yamijala, S. S. R. K. C.; Shinde, R.; Wong, B. M. Real-time degradation dynamics of hydrated per- and polyfluoroalkyl substances (PFASs) in the presence of excess electrons. *Phys. Chem. Chem. Phys.* **2020**, *22*, 6804−6808.

(13) Bentel, M. J.; Yu, Y.; Xu, L.; Li, Z.; Wong, B. M.; Men, Y.; Liu, J. Defluorination of per- and polyfluoroalkyl substances (PFASs) with hydrated electrons: structural dependence and implications to PFAS remediation and management. *Environ. Sci. Technol.* **2019**, *53*, 3718−3728.

(14) Su, Y.; Rao, U.; Khor, C. M.; Jensen, M. G.; Teesch, L. M.; Wong, B. M.; Cwiertny, D. M.; Jassby, D. Potential-driven electron transfer lowers the dissociation energy of the C−F bond and facilitates reductive defluorination of perfluorooctane sulfonate (PFOS). *ACS Appl. Mater. Interfaces* **2019**, *11*, 33913−33922.

(15) Maza, W. A.; Breslin, V. M.; Owrutsky, J. C.; Pate, B. B.; Epshteyn, A. Nanosecond transient absorption of hydrated electrons and reduction of linear perfluoroalkyl acids and sulfonates. *Environ. Sci. Technol. Lett.* **2021**, *8*, 525−530.

(16) Xu, T.; Zhu, Y.; Duan, J.; Xia, Y.; Tong, T.; Zhang, L.; Zhao, D. Enhanced photocatalytic degradation of perfluorooctanoic acid using carbon-modified bismuth phosphate composite: effectiveness, material synergy and roles of carbon. *Chem. Eng. J.* **2020**, *395*, 124991.

(17) Duan, L.; Wang, B.; Heck, K. N.; Clark, C. A.; Wei, J.; Wang, M.; Metz, J.; Wu, G.; Tsai, A.-L.; Guo, S.; Arredondo, J.; Mohite, A. D.; Senftle, T. P.; Westerhoff, P.; Alvarez, P.; Wen, X.; Song, Y.; Wong, M. S. Titanium oxide improves boron nitride photocatalytic degradation of perfluorooctanoic acid. *Chem. Eng. J.* **2022**, *448*, 137735.

(18) James Wood, R.; Sidnell, T.; Ross, I.; McDonough, J.; Lee, J.; Bussemaker, M. J. Ultrasonic degradation of perfluorooctane sulfonic acid (PFOS) correlated with sonochemical and sonoluminescence characterisation. *Ultrason. Sonochem.* **2020**, *68*, 105196.

(19) Sharma, S.; Shetti, N. P.; Basu, S.; Nadagouda, M. N.; Aminabhavi, T. M. Remediation of per- and polyfluoroalkyls (PFAS) via electrochemical methods. *Chem. Eng. J.* **2022**, *430*, 132895.

(20) Zhang, H.; Li, P.; Zhang, A.; Sun, Z.; Liu, J.; Héroux, P.; Liu, Y. Enhancing interface reactions by introducing microbubbles into a plasma treatment process for efficient decomposition of PFOA. *Environ. Sci. Technol.* **2021**, *55*, 16067−16077.

(21) Gu, Y.; Liu, T.; Zhang, Q.; Dong, W. Efficient decomposition of perfluorooctanoic acid by a high photon flux UV/sulfite process: kinetics and associated toxicity. *Chem. Eng. J.* **2017**, *326*, 1125−1133.

(22) Wang, F.; Lu, X.; Shih, K.; Liu, C. Influence of calcium hydroxide on the fate of perfluorooctanesulfonate under thermal conditions. *J. Hazard. Mater.* **2011**, *192*, 1067−1071.

(23) Wang, F.; Shih, K.; Lu, X.; Liu, C. Mineralization behavior of fluorine in perfluorooctanesulfonate (PFOS) during thermal treatment of lime-conditioned sludge. *Environ. Sci. Technol.* **2013**, *47*, 2621−2627.

(24) Wang, F.; Lu, X.; Li, X.-y.; Shih, K. Effectiveness and mechanisms of defluorination of perfluorinated alkyl substances by calcium compounds during waste thermal treatment. *Environ. Sci. Technol.* **2015**, *49*, 5672−5680.

(25) Wang, N.; Lv, H.; Zhou, Y.; Zhu, L.; Hu, Y.; Majima, T.; Tang, H. Complete defluorination and mineralization of perfluorooctanoic acid by a mechanochemical method using alumina and persulfate. *Environ. Sci. Technol.* **2019**, *53*, 8302−8313.

(26) Yuan, Y.; Feng, L.; He, X.; Liu, X.; Xie, N.; Ai, Z.; Zhang, L.; Gong, J. Efficient removal of PFOA with an In$_2$O$_3$/persulfate system under solar light via the combined process of surface radicals and photogenerated holes. *J. Hazard. Mater.* **2022**, *423*, 127176.

(27) Biswas, S.; Wong, B. M. High-temperature decomposition of diisopropyl methylphosphonate on alumina: mechanistic predictions from ab initio molecular dynamics. *J. Phys. Chem. C* **2021**, *125*, 21922−21932.

(28) Vasudevan, A.; Senyurt, E. I.; Schoenitz, M.; Dreizin, E. L. Removal of diisopropyl methyl phosphonate (DIMP) from heated metal oxide surfaces. *J. Hazard. Mater.* **2023**, *443*, 130154.

(29) VandeVondele, J.; Hutter, J. An efficient orbital transformation method for electronic structure calculations. *J. Chem. Phys.* **2003**, *118*, 4365−4369.

(30) Perdew, J. P.; Burke, K.; Ernzerhof, M. Generalized gradient approximation made simple. *Phys. Rev. Lett.* **1996**, *77*, 3865−3868.

(31) Grimme, S. Semiempirical GGA-type density functional constructed with a long-range dispersion correction. *J. Comput. Chem.* **2006**, *27*, 1787−1799.

(32) Goedecker, S.; Teter, M.; Hutter, J. Separable dual-space Gaussian pseudopotentials. *Phys. Rev. B* **1996**, *54*, 1703−1710.

(33) Hartwigsen, C.; Goedecker, S.; Hutter, J. Relativistic separable dual-space Gaussian pseudopotentials from H to Rn. *Phys. Rev. B* **1998**, *58*, 3641−3662.

(34) Nosé, S. A unified formulation of the constant temperature molecular dynamics methods. *J. Chem. Phys.* **1984**, *81*, 511−519.

(35) Hoover, W. G. Canonical dynamics: equilibrium phase-space distributions. *Phys. Rev. A* **1985**, *31*, 1695−1697.

(36) Digne, M.; Sautet, P.; Raybaud, P.; Euzen, P.; Toulhoat, H. Hydroxyl groups on γ-alumina surfaces: a DFT study. *J. Catal.* **2002**, *211*, 1−5.

(37) Digne, M.; Sautet, P.; Raybaud, P.; Euzen, P.; Toulhoat, H. Use of DFT to achieve a rational understanding of acid−basic properties of γ-alumina surfaces. *J. Catal.* **2004**, *226*, 54−68.

(38) Wilson, S. The dehydration of boehmite, γ-AlOOH, to γ-Al_2O_3. *J. Solid State Chem.* **1979**, *30*, 247−255.

(39) Wischert, R.; Copéret, C.; Delbecq, F.; Sautet, P. Optimal water coverage on alumina: a key to generate Lewis acid−base pairs that are reactive towards the C-H bond activation of methane. *Angew. Chem., Int. Ed.* **2011**, *50*, 3202−3205.

(40) Joubert, J.; Salameh, A.; Krakoviack, V.; Delbecq, F.; Sautet, P.; Copéret, C.; Basset, J. M. Heterolytic splitting of H_2 and CH_4 on γ-alumina as a structural probe for defect sites. *J. Phys. Chem. B* **2006**, *110*, 23944−23950.

(41) Deng, X.; Herranz, T.; Weis, C.; Bluhm, H.; Salmeron, M. Adsorption of water on Cu_2O and Al_2O_3 thin films. *J. Phys. Chem. C* **2008**, *112*, 9668−9672.